doi:10.1093/brain/awv284 BRAIN 2015: 138; 3520–3536 | 3520

BRAIN
A JOURNAL OF NEUROLOGY

Alteration in 5-hydroxymethylcytosine-mediated epigenetic regulation leads to Purkinje cell vulnerability in ATM deficiency

Dewei Jiang,[1,2] Ying Zhang,[1] Ronald P. Hart,[3] Jianmin Chen,[3] Karl Herrup[4] and Jiali Li[1]

A long-standing mystery surrounding ataxia-telangiectasia is why it is mainly cerebellar neurons, Purkinje cells in particular, that appear vulnerable to ATM deficiency. Here we present data showing that 5-hydroxymethylcytosine (5hmC), a newly recognized epigenetic marker found at high levels in neurons, is substantially reduced in human ataxia-telangiectasia and $Atm^{-/-}$ mouse cerebellar Purkinje cells. We further show that TET1, an enzyme that converts 5-methylcytosine (5mC) to 5hmC, responds to DNA damage and manipulation of TET1 activity directly affects the DNA damage signalling and ATM-deficient neuronal cell cycle re-entry and death. Quantitative genome-wide analysis of 5hmC-containing sequences shows that in ATM deficiency there is a cerebellum- and Purkinje cell-specific shift in 5hmC enrichment in both regulatory elements and repeated sequences. Finally, we verify that TET1-mediated 5hmC production is linked to the degenerative process of Purkinje cells and behavioural deficits in $Atm^{-/-}$ mice. Taken together, the selective loss of 5hmC plays a critical role in driving Purkinje cell vulnerability in ATM deficiency.

1 Key Laboratory of Animal Models and Human Disease Mechanisms of Chinese Academy of Sciences and Yunnan Province, Kunming Institute of Zoology, Kunming, Yunnan, 650223, China
2 Kunming College of Life Science, University of Chinese Academy of Sciences, Kunming 650223, China
3 Department of Cell Biology and Neuroscience, Rutgers University, Piscataway, NJ, USA
4 Division of Life Science and the State Key Laboratory of Molecular Neuroscience, The Hong Kong University of Science and Technology, Clear Water Bay, Kowloon, Hong Kong

Correspondence to: Jiali Li,
Key Laboratory of Animal Models and Human Disease Mechanisms of Chinese Academy of Sciences and Yunnan Province,
Kunming Institute of Zoology,
Kunming, Yunnan, 650223,
China
E-mail: lijiali@mail.kiz.ac.cn

Keywords: DNA demethylation; Purkinje cell vulnerability; ataxia-telangiectasia; 5-hydroxymethylcytosine; TET1

Abbreviations: 5hmC = 5-hydroxymethylcytosine; 5mC = 5-methylcytosine; GFP = green fluorescent protein

Introduction

Ataxia-telangiectasia is a hereditary multisystemic disease resulting from mutations in the *ATM* gene. Part of the complexity of ataxia-telangiectasia neurological symptoms is the high degree of cell type specificity among neuronal subtypes. Neuropathological and imaging studies suggest that cerebellar neurons are particular targets of ataxia-telangiectasia—most especially the cerebellar Purkinje cell. Although a high requirement for energy metabolism may contribute to Purkinje cell vulnerability (Chakrabarti *et al.*, 2010), the same might well be applied to other neuronal

Received February 27, 2015. Revised July 21, 2015. Accepted August 5, 2015. Advance Access publication October 28, 2015

cell types in the CNS and thus the mechanism of Purkinje cell vulnerability in ATM deficiency remains unknown.

Aberrant DNA methylation followed by abnormal gene expression was first reported as an epigenetic hallmark of cancer (Haffner *et al.*, 2011; Malzkorn *et al.*, 2011). The methylation of the cytosine base *in situ* to produce 5-methylcytosine (5mC) is catalysed by DNA methyltransferases (Lian *et al.*, 2012). It is estimated that ~2–8% of the total cytosines in human genomic DNA are 5mC. This modification impacts a broad range of biological functions, including gene expression, maintenance of genome integrity, parental imprinting, X-chromosome inactivation, regulation of development, ageing and cancer.

The question of whether and how DNA is demethylated has only recently been addressed. Ten-eleven translocation proteins (TET1–TET3), which are 180–235 (kD) dioxygenases for demethylating 5mC, have an enzymatic activity that converts 5mC to 5-hydroxymethylcytosine (5hmC) (Tahiliani *et al.*, 2009; Kudo *et al.*, 2012). This oxidized form of 5mC is known as the 'sixth base'. Its presence adds a layer of complexity to the epigenetic regulation of DNA methylation (Tahiliani *et al.*, 2009; Ito *et al.*, 2010) and has been found in a variety of mammalian cells, in particular in self-renewing and pluripotent stem cells and neuronal cells (Szwagierczak *et al.*, 2010; Guo *et al.*, 2011). Currently, the biological role of 5hmC is not fully understood; but it has been suggested to have potential as a cancer biomarker and is believed, like 5mC, to play an important role in switching genes on and off. Through correlations with defined chromatin signatures at promoter and enhancer subtypes, a distinct enrichment of 5hmC at enhancers marked with H3K4me3 (histone 3 lysine 4 trimethylation) and H3K27ac (histone H3 acetyl Lys27) suggests a potential role for 5hmC in the regulation of the pluripotency and differentiation of embryonic stem cells (Pastor *et al.*, 2011; Szulwach *et al.*, 2011*a*; Yu *et al.*, 2012). This finding indicates that multiple epigenetic systems may have correlated effects in a single biological or pathological process. Of particular significance to our study is the finding of large differences of 5hmC content among different cells in different tissues.

In mice and in humans, the percentage of 5hmC is particularly high in the brain relative to other tissues (Kriaucionis and Heintz, 2009; Globisch *et al.*, 2010; Li and Liu, 2011). Estimates suggest that it accounts for ~40% of the modified cytosine in brain and has been suggested to play a role in neuronal plasticity (Szulwach *et al.*, 2011*b*). Low levels of 5hmC have also been associated with brain tumour differentiation and anaplasia (Kraus *et al.*, 2012; Lian *et al.*, 2012). While 5mC suppresses transcription by recruiting repressors to gene promoters (Deaton and Bird, 2011), the function of 5hmC is less certain. In the mouse cortex and cerebellum, 5hmC is enriched within genes and appears to promote gene transcription levels (Jin *et al.*, 2011; Song *et al.*, 2011). Although it is thought of as an intermediate state of complete DNA demethylation, 5hmC can also affect genomic function by blocking binding of transcription repressors (Guo *et al.*, 2011; He *et al.*, 2011; Ito *et al.*, 2011; Zhang *et al.*, 2012). Synchronous neuronal activity promotes active DNA demethylation of plasticity-related genes in the mouse brain through TET-mediated formation of 5hmC (Guo *et al.*, 2011); however, it is not known whether such demethylation completely accounts for the enrichment of 5hmC in the brain. What is known is that DNA methylation and demethylation are dynamic, their levels influence brain function and they are altered in neurological disorders (Chia *et al.*, 2011). Genome-wide mapping of 5hmC in mouse hippocampus and cerebellum has indicated an increase of 5hmC with age in the mouse brain as well as an age- and gene expression level-related enrichment of 5hmC in genes implicated in neurodegeneration (Szulwach *et al.*, 2011*b*).

Our previous studies have demonstrated that nuclear accumulation of HDAC4 (Li *et al.*, 2012), and EZH2 stabilization (Li *et al.*, 2013) both contribute to ataxia-telangiectasia neurodegeneration by altering the histone acetylation and methylation status of the genome, respectively. As the genome of all neurons carries the identical *ATM* mutation, the question arises as to whether there are additional epigenetic factors, such as DNA methylation, that play a role in driving specific disease mechanisms. Purkinje cells are among the largest cells in the brain. Purkinje cell nuclei are large and pale, and the majority of heterochromatin detectable at the ultrastructural level is present surrounding the large, centrally located nucleolus. The levels of 5hmC in Purkinje cell are much higher than in granule cell nuclei, suggesting that 5hmC may have a particularly important role in Purkinje cell function (Kriaucionis and Heintz, 2009).

We report here that 5hmC is substantially reduced in human ataxia-telangiectasia and $Atm^{-/-}$ mouse cerebellar Purkinje cells. TET1-mediated conversion of 5mC to 5hmC responds to DNA damage in an ATM-dependent manner. Manipulation of TET1 activity directly affects the subsequent DNA damage signalling, cell cycle re-entry and cell death. In ATM deficiency there is a genome-wide reduction and shift of 5hmC 'marks' at both regulatory elements and repeat sequences in cerebellar cortex but not in frontal cortex. Finally, we validate that TET1 activity links to the degenerative process in Purkinje cells as well as behavioural deficits in $Atm^{-/-}$ mice. Our work suggests that in ATM deficiency, loss of 5hmC contributes to a Purkinje cell-enriched epigenetic alteration that deregulates chromatin structure and alters gene expression as well as DNA damage signalling.

Materials and methods

Isolation of Purkinje cells

Isolation of Purkinje cells was performed as described (Tomomura *et al.*, 2001) with modification. Briefly, cerebella were removed from 2-month-old wild-type and $Atm^{-/-}$ mutant

mice. Cubes of cerebella (0.5-mm) were digested at 37°C for 15 min with 0.025% trypsin in dissociation solution. The reaction was stopped by the addition of one volume of dissociation solution containing 0.25 mg/ml soybean trypsin inhibitor and DNase I (40 µg/ml). Tissues were triturated mildly by sequentially passage through 5 ml pipettes. After the cells were filtered through a 35 µm cell strainer, they were resuspended in Ca^{2+}- and Mg^{2+}-free dissociation solution. The single-cell suspension was then incubated with FITC-labelled NMDA-NR1 antibody for 1 h at room temperature. After washing three times, PI (Sigma-Aldrich) was added to label the dead cells. Cell sorting was performed with the FACS BD LSRFortessa (BD). The isolated Purkinje cells were centrifuged at 200*g* for 5 min and prepared for genomic DNA extraction [FITC-labelled NMDA-NR1 antibody was labelled with FITC Conjugation Kit (Abcam)].

Cerebellar slice cultures and viral infection

Whole brains of postnatal Day 3 wild-type and *Atm*$^{-/-}$ mice were dissected out into Eagle's medium with Earle's salts medium (MEM). Sagittal slices (350 µm) of the cerebellum were cut using a McIlwain tissue chopper. Two to three slices were plated onto each Millipore Millicell-CM™ organotypic culture insert, and the inserts were placed in a 6-well plate containing 1 ml serum-free slice culture medium and cultured at 37°C in 5% CO_2. Medium was changed every 3 days. Serum-free slice culture medium consists of Neurobasal® A medium, B27 supplement, 2.5 mM L-glutamine and 5 mM glucose. All media contained 100 U/ml penicillin and 100 µg/ml streptomycin. For slice viral infection, 1 µl of lentiviral particles ($1–5 \times 10^9$ TU/ml) and 1 µl adenoviral particles ($1–3 \times 10^{13}$ TU/ml) were added to the medium immediately before slices were plated and removed when the medium was replaced. Two weeks after viral infection, slices were fixed with 4% paraformaldehyde, blocked with 5% heat-inactivated goat serum and 0.25% Tween-20, and then incubated in primary antibodies overnight at 4°C. Staining was visualized by incubation in appropriate secondary antibodies at room temperature.

Genomic DNA preparation and dot blot

Genomic DNA was isolated from wild-type and *Atm*$^{-/-}$ adult mouse cortex, cerebellum and isolated Purkinje cells with PureLink™ Genomic DNA Purification kits (Invitrogen). Purified genomic DNA was sonicated to produce fragments of ~200–500 bp in length (Bioruptor). Dot blots were performed on a Bio-Dot Apparatus as described previously using rabbit antibody to 5hmC (#39769, Active Motif) as the primary antibody, incubated overnight at 4°C. Horseradish peroxidase–conjugated antibody to rabbit (Sigma) was used as a secondary antibody, and incubated for 30 min at 20–25°C. Standard DNA templates were loaded for the quantification and to verify the specificity of antibodies.

5hmC and hydroxymethylated DNA immunoprecipitation sequencing

Genomic DNA was purified from human control and ataxia-telangiectasia cerebellar cortex as well as isolated mouse Purkinje cells and sonicated. 5hmC or 5mC was immunoprecipitated as described (Guo *et al.*, 2011). Briefly, 15–20 µg of each sonicated DNA was diluted to 300 µl in Tris–EDTA buffer (pH 8.0), and denatured for 10 min in boiling water and immediately cooled on ice for 10 min. Then, 34 µl of 10 × immunoprecipitation buffer [100 mM sodium phosphate (pH 7.0) 1.4 M NaCl, 0.5% Triton™ X-100] and 2 µg of 5hmC or 5mC antibody (Active Motif) were added to each sample, followed by overnight incubation at 4°C. Dynabeads protein G (Invitrogen) pre-blocked with 0.5% bovine serum albumin in phosphate-buffered saline were added to pull down antibody-DNA complexes for 2 h at 4°C. Beads were washed three times with immunoprecipitation buffer, resuspended in 400 µl of proteinase K digestion solution [50 mM Tris-HCl pH 8.0, 10 mM EDTA, 0.5% sodium dodecyl sulphate, 0.2 mg/ml proteinase K] and incubated on a 50°C shaker for 3 h. DNA was extracted with Qiagen purification kit and dissolved in Tris–EDTA buffer (pH 8.0).

For 5hmC sequencing, DNA was amplified using an Illumina TruSeq DNA Sample kit. A total of 0.5–1 µg DNA was used for each experiment. Input samples were produced for each cell type ($n = 2$). 5mC- ($n = 1$) and 5hmC-enriched ($n = 3$) libraries were then sequenced using Illumina HiSeq 2500 platform obtaining more than 6×10^6 reads per sample. Reads were aligned with hg19 human genome using Bowtie (Langmead *et al.*, 2009). Enriched broad peaks were identified using MACS2 (Feng *et al.*, 2012). Identification of enriched intervals overlapping CpG islands (obtained from the UCSC Genome Browser) was done using bedtools (Quinlan and Hall 2010). Transcription unit plotting was performed with NGS-Plot software (Shen *et al.*, 2014). Data have been deposited in the NIH GEO repository, accession number GSE61169.

Illumina microarrays

RNA samples were run on Illumina HT-12v4.0 microarrays at the Sanford Burnham Medical Research Institute. Results were modelled in limma (Smyth, 2005), and probe identifiers were translated to gene symbols using biomaRt. Data have been deposited in the NIH GEO repository, accession number GSE61169.

Virus production and cerebellar injections

Viral preparation and cerebellar microinjection were conducted as previously described (Li *et al.*, 2012, 2013). Briefly, premade lentiviral constructs including a set of *Tet1–3* short hairpin (sh) RNAs were from Sigma (Supplementary Table 1). The high adenoviral TET1 wild-type and kinase inactivated mutant (KD) viral particle titres were prepared with an adenoviral expression system and purified by Adenoviral Purification Kits (Applied Biological Material Inc.). Stereotaxic intracerebellar infusions were delivered to wild-type and *Atm*$^{-/-}$ mice (8 weeks of age). For each cerebellum, slow infusion over 15 min of 3–5 µl of lentiviral

particles ($1–5 \times 10^9$ TU/ml) or 2–3 µl adenoviral particles ($1–3 \times 10^{13}$ TU/ml), was performed. For knocking down endogenous mouse TET1 and overexpressing human TET1, we delivered short hairpin *TET1* (*shtet1*) lentivirus: human TET1 adenoviruses as 1:1 ratio in 2-month-old mice. After surgery, animals were injected subcutaneously with 0.3 ml prewarmed saline to avoid dehydration, and were allowed 7 days recovery prior to tissue collection. For behavioural experiments, viruses were injected into mouse cerebellum at postnatal Day 18, and 3 weeks later, trained for tests of motor behaviour.

Behavioural test

The rota-rod and open-field test was conducted as previously described (Li *et al.*, 2012, 2013).

Statistical analyses

All non-behavioural data are presented as the means ± standard error of the mean (SEM) of a minimum of three replicates. With the exception of the behavioural data, we evaluated statistical differences by Student's *t*-test. Behavioural data were analysed by two-way ANOVAs, with repeated measures included for the open field data. *Post hoc* testing used Neuman-Keuls or Bonferroni *t*-tests where appropriate. Effects were considered significant at $P < 0.05$.

Results

Loss of 5hmC in ATM-deficient Purkinje cells

To explore whether the abundance of 5hmC is related to Purkinje cell viability, we examined the levels of 5mC and 5hmC in Purkinje cells in human cerebellum from four pairs of individuals, one of whom died with no known brain disease, the other with a diagnosis of ataxia-telangiectasia. In control cerebellum, as predicted, the level of 5hmC is relatively high in Purkinje cells (Fig. 1A, B and Supplementary Fig. 1A). By contrast, in ataxia-telangiectasia cerebellum, the levels of 5hmC in Purkinje cells were significantly reduced ($P < 0.05$). The levels of 5mC in Purkinje cells, in both control and ataxia-telangiectasia cerebellum, revealed few alterations (Supplementary Fig. 1B).

Although most *Atm* mutant mice lack frank cerebellar neurodegeneration, we and other groups have documented Purkinje cell degenerative events in the $Atm^{-/-}$ ($Atm^{tm1Bal/tm1Bal}$) cerebellum (Kuljis *et al.*, 1997; Li *et al.*, 2011). To assess whether loss of 5hmC in human ataxia-telangiectasia Purkinje cells could also be found in $Atm^{-/-}$ mouse brain, we examined the levels of 5hmC in several brain regions in both wild-type and $Atm^{-/-}$ adult mice. As in the human ataxia-telangiectasia samples, the intensity of 5hmC in Purkinje cells was remarkably decreased in mutant mice in comparison to wild-type (Fig. 1A and B). By contrast, few alterations were found in the levels of 5hmC in granule cells or in neurons of other brain regions such as neocortex and hippocampus (Supplementary Fig. 1B and C). Again, 5mC showed little change in $Atm^{-/-}$ neurons (Supplementary Fig. 1B and C).

To confirm the selective loss of 5hmC in ATM-deficient Purkinje cells, we decided to determine the total amount of 5hmC and 5mC in isolated Purkinje cells from wild-type and $Atm^{-/-}$ adult mice through a dot-blot assay. NMDA-NR1, the NMDA receptor subtype R1 (encoded by *GRIN1*), with high expression levels in Purkinje cells, has been used as a Purkinje cell-specific membrane marker (Thompson *et al.*, 2000). For collection of Purkinje cells, we isolated live Purkinje cells by directly labelling surface NR1 receptors with an FITC-labelled NR1 antibody followed by fluorescence-activated cell sorting (FACS) (Supplementary Fig. 2A). Aldolase C and calbindin were examined for identification of isolated Purkinje cells (Supplementary Fig. 2B and C). We then determined the total amount of 5hmC in isolated Purkinje cells as well as in extracts of whole neocortex and cerebellar cortex from wild-type and $Atm^{-/-}$ adult mice. Assaying whole cerebral cortex, we found that the amount of 5hmC was nearly identical in wild-type and $Atm^{-/-}$ mice. In whole cerebellar cortex we noted a slight decrease in $Atm^{-/-}$ cerebellar samples, although this difference was not significant. By contrast in our isolated Purkinje cell samples, we observed a significant reduction of the amount of 5hmC in $Atm^{-/-}$ compared to wild-type, however, the levels of 5mC revealed few alterations in ATM deficiency (Fig. 1C, D and Supplementary Fig. 1D and E). This observation suggests that ATM deficiency mainly leads to the selective loss of 5hmC in Purkinje cells.

As TETs are the enzymes responsible for converting 5mC to 5hmC, we therefore asked whether loss of 5hmC in ATM-deficient Purkinje cells was related to TETs. We examined the level of all three TET protein isoforms: TET1, TET2 and TET3. Despite the substantial change in the levels of 5hmC, there was no significant decrease in any of the isoforms, either in immunocytochemistry preparations or on western blots (Fig. 1E, Supplementary Fig. 1B and C). The levels of *TET1*, *TET2* and *TET3* mRNA were also fairly constant (Fig. 1F). These results suggest that the loss of 5hmC in ataxia-telangiectasia Purkinje cells may be the result of deregulated TET enzymatic activity.

TET1 is an ATM target

To explore which TET was most involved in the loss of 5hmC in ATM deficiency, first, we determined whether TET1, 2 or 3 responded to ATM-dependent DNA damage signalling. Protein was extracted from cerebellar cortex of adult wild-type mice that were either untreated or exposed to whole body γ-irradiation (5 Gy) followed by a 6-h recovery period. We then immunoprecipitated TET1, TET2 and TET3 and probed a western blot of the precipitate with an antibody that recognizes phosphorylated serine or threonine residues followed by a glutamine residue (^{P}[S/

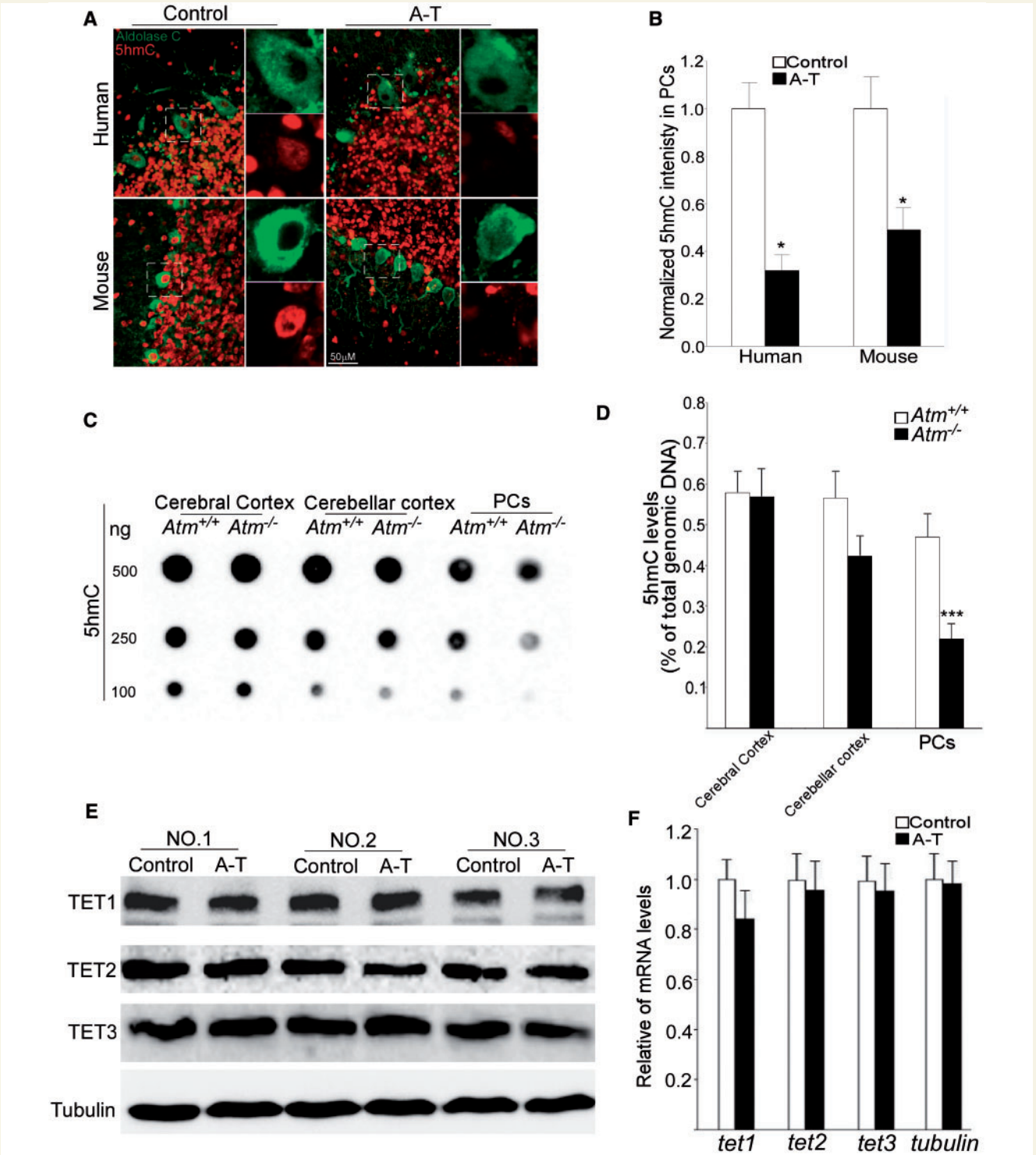

Figure 1 Selective loss of 5hmC found in human ataxia-telangiectasia and *Atm*$^{-/-}$ mice cerebellar Purkinje cells. (**A**) Paraffin sections of control and ataxia-telangiectasia (A-T) human cerebellum as well as 10 μm cryostat sections of wild-type and *Atm*$^{-/-}$ mice brains were immunostained with 5hmC (red). Aldolase C immunostaining (green) was used as a marker of Purkinje cells (PCs). (**B**) The normalized intensity of 5hmC staining illustrated in **A**. Five to eight images per slide; three slides per patient. Data are presented as mean ± SEM. (n = 3–5 patient or mice). *$P < 0.001$, one-way ANOVA. Scale bar = 50 μm. (**C**) 5hmC-specific dot-blot intensities of genomic DNA isolated from the neocortex, cerebellar cortex as well as isolated Purkinje cells of *Atm*$^{+/+}$ and *Atm*$^{-/-}$ adult mice. (**D**) Global 5hmC levels in *Atm*$^{+/+}$ and *Atm*$^{-/-}$mice brain were quantified using 5hmC-specific dot-blot intensities. Amounts of 5hmC are shown as a percentage of total nucleotides in the genome, which are quantified from 5hmC-specific dot-blot intensities normalized to positive controls. (*$P < 0.05$, Student's t-test; mean ± SEM; n = 3–5 per each type of mouse). (**E** and **F**) The levels of TET1, 2 and 3 protein and mRNA showed little change in control and ataxia-telangiectasia cerebellar cortex. Protein and total RNA were extracted from human cerebellar cortex.

T]Q), the canonical ATM kinase target sequence. Immunoprecipitated TET1, but not TET2 or TET3, showed a strong ^{P}[S/T]Q band after γ-irradiation (Fig. 2A and B). To validate this finding, green fluorescent protein-tagged TET1 (GFP-TET1) was transfected into neuronal N2a cells. Two days later the transfected cells were exposed to 10 μM etoposide treatment for 1 h. GFP immunoprecipitates were prepared and western blots examined with ^{P}[S/T]Q antibody. Robust ^{P}[S/T]Q signals on GFP-TET1 as well as GFP-EZH2 were found after etoposide treatment (Fig. 2C). Next, to examine whether ATM-mediated TET1 phosphorylation is present *in vivo*, first, we immunoprecipitated TET1 from lysates of human and mouse cerebellar cortex tissues and probed the resulting western blots with ^{P}[S/T]Q antibody. In both control human and wild-type mouse cerebellar cortex, the immunoprecipitated TET1 gave a ^{P}[S/T]Q band on western blots (Fig. 2D). By contrast, lysates from ataxia-telangiectasia patient and *Atm*$^{-/-}$ mice had little to no detectable ^{P}[S/T]Q reactivity. Analysis of the TET1 protein sequence predicts that S116, S262 and S546 are highly probable sites of ATM phosphorylation. We therefore verified that S116 is the predominant ATM site on TET1 by performing ATM *in vitro* kinase assays using GST-TET1 fusion proteins as substrates (Fig. 2E). The phosphorylation signal was nearly lost when the TET1-S116A mutant was used as substrate; the 3SA (S116A/S262A/S546A) triple mutation blocked the phosphorylation signal entirely. This indicates that S116 is the major ATM phosphorylation site, but S262 and S546 may serve as alternate kinase sites. To confirm this finding, GFP-TET1 wild-type or non-phosphorylatable mutant 3SA were co-transfected with Flag-ATM wild-type (WT) and kinase dead mutant (KD) into *Atm*$^{-/-}$ mouse embryonic fibroblasts. Two days later the transfected cells were exposed to 10 μM etoposide treatment for 1 h. GFP-TET1 immunoprecipitates were prepared and western blots examined with ^{P}[S/T]Q antibody. A strong ^{P}[S/T]Q signal was found with etoposide treatment when GFP-TET1-WT was expressed with Flag-ATM-WT (Fig. 2F). Expression of either the GFP-TET1-3SA mutant or the Flag-ATM-KD mutant significantly reduced the response. Interestingly, an interaction of GFP-TET1-WT with Flag-ATM-WT was also found after etoposide treatment. However, these phenotypes were not found in GFP-TET1-3SA or Flag-ATM-KD transfected cells (Fig. 2F). Next, to test whether 5hmC levels are directly affected by the phosphorylation of TET1 by ATM in DNA damage response, GFP-TET1-WT and 3SA were co-transfected with Flag-ATM-WT into *Atm*$^{-/-}$ mouse embryonic fibroblasts. The amount of 5hmC is examined through dot blot assay. Increased levels of 5hmC were found in *Atm*$^{-/-}$ mouse embryonic fibroblasts with GFP-TET1-WT and Flag-ATM co-transfected cells, however, overexpression of 3SA with Flag-ATM has little effect on 5hmC levels (Fig. 2G and H). These data indicate that TET1 is a new ATM target and is likely to participate in the DNA damage response.

5hmC levels respond to DNA damage

TET-dependent conversion of 5mC to 5hmC has been discovered only recently (Tahiliani *et al.*, 2009; Chaudhry and Omaruddin, 2012), and the factors that regulate TET activity remain unknown in most biological processes. To assess whether TET1 activity responds to DNA damage in an ATM-dependent manner, we treated primary mouse cortical neurons grown in culture for 10 days from wild-type (*Atm*$^{+/+}$) and *Atm*$^{-/-}$ mice with 10 Gy γ-irradiation. Three hours later, the cultures were fixed with 4% paraformaldehyde and stained for 5mC or 5hmC. Irradiation produced a dramatic increase of 5hmC intensity in wild-type neurons; in *Atm*$^{-/-}$ neurons, by contrast, there was little change (Fig. 3A and B). This response to DNA damage was not restricted to neurons. We conducted a similar experiment in human fibroblast cells and found that after irradiation, the levels of 5hmC were elevated in control cells but not in cells from patients with ataxia-telangiectasia (Supplementary Fig. 3A and B). The observation is most likely due directly to DNA damage rather than some other side effect of the radiation as similar results were found after treatment with the topoisomerase inhibitor, etoposide, in the HT22 neuronal cell line (Fig. 3C and D). Unexpectedly, robust number and increased size of nuclear foci of TET1 were also induced by DNA damage in control fibroblasts (Supplementary Fig. 3C). While little change of 5mC were found in ataxia-telangiectasia brain (Supplementary Fig.1B–E), the 5mC levels changed in the opposite direction from those of 5hmC in DNA damage response (Fig. 3C, D and Supplementary Fig. 3A and B).

This indicates that DNA damage directly leads to DNA demethylation in an active manner by which the inability to convert 5mC to 5hmC might lead to a build-up of the 5mC substrate.

To confirm these findings, we determined whether DNA damage leads to alteration in the total amount of 5hmC through a dot blot assay. The amount of 5hmC is significantly increased in wild-type mouse embryonic fibroblasts after γ-irradiation treatment; however, little alteration of 5hmC levels was found in *Atm*$^{-/-}$ mouse embryonic fibroblasts (Fig. 3E and F). Next, GFP-TET1 was co-transfected with Flag-ATM-WT and -KD into *Atm*$^{-/-}$ mouse embryonic fibroblasts; 2 days later, the transfected mouse embryonic fibroblasts were exposed to γ-irradiation. As expected, a significant increase of the amount of 5hmC was found in the overexpression of GFP-TET1 and Flag-ATM-WT after γ-irradiation. However, little alteration of 5hmC levels was found in *Atm*$^{-/-}$ mouse embryonic fibroblasts with overexpressed GFP-TET1 and Flag-ATM-KD. Interestingly, introduction of TET1 CRISPR/Cas9 knockout plasmid, GFP fusion Cas9-Tet1, led to a decreased 5hmC due to loss of TET1 function (Fig. 3E and F). Our observation suggests that TET1-mediated 5hmC responds to DNA damage in an ATM-dependent way.

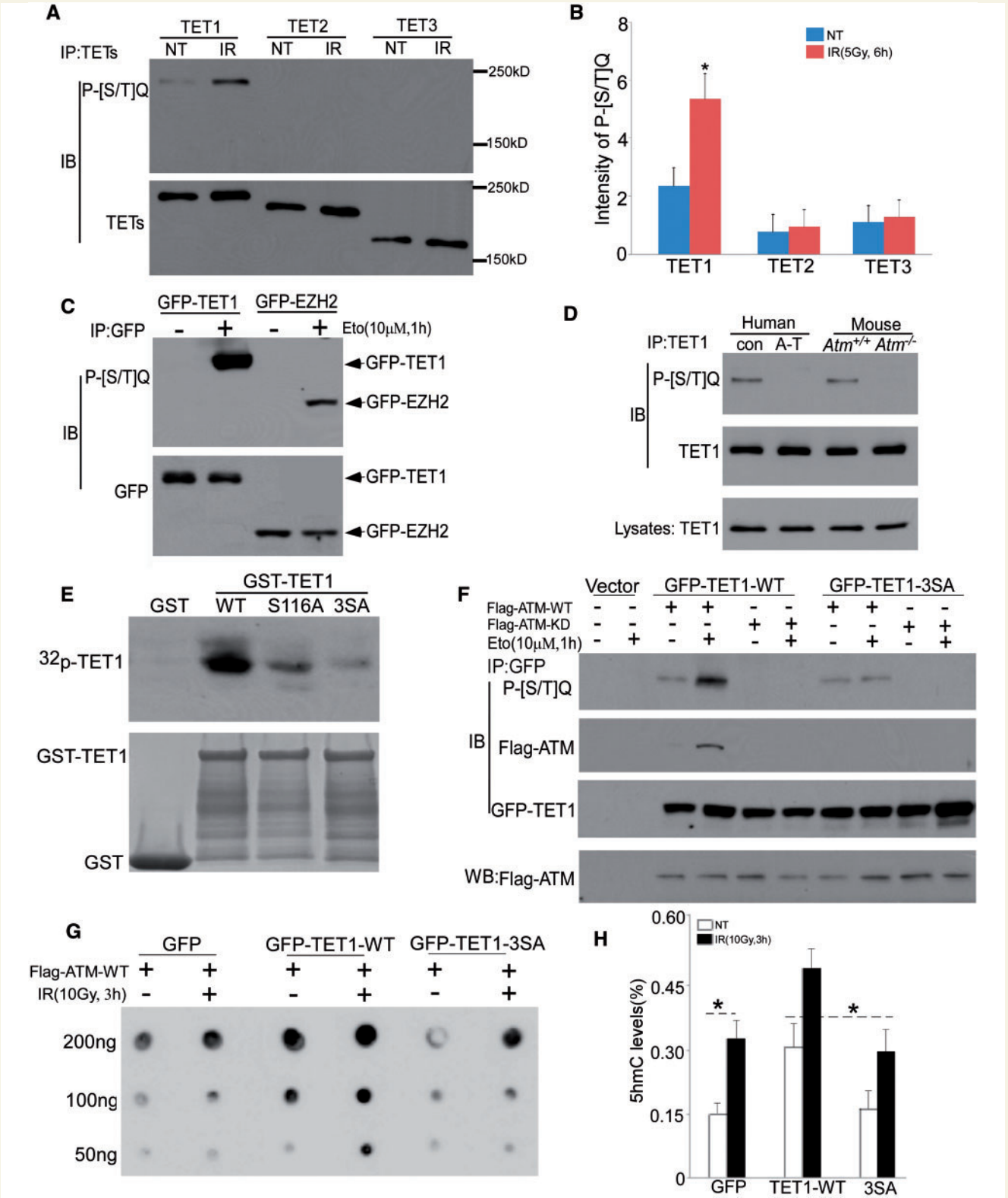

Figure 2 TET1 is a target of ATM. (**A**) Protein extracts from adult wild-type mice cerebellar cortex were immunoprecipitated with the TET1, TET2 and TET3 and blotted with the ^{P}[S/T]Q antibody to detect ATM-like kinase activity. (**B**) Quantification of three repetitions of the experiment illustrated in **A**. Error bars denotes standard deviations. *$P < 0.05$ (by Student's *t*-test). (**C**) GFP-TET1 and GFP-EZH2 were expressed in N2a cells. GFP immunoprecipitates were blotted with anti-GFP or anti-^{P}[S/T]Q. GFP-EZH2 served as a positive control for ATM phosphorylation. (**D**) Protein extracts from frozen human and mouse cerebellar cortex tissues were immunoprecipitated with the TET1 antibody and blotted with the ^{P}[S/T]Q antibody. (**E**) *In vitro* ATM kinase. N2a cell extract (100 μg) was immunoprecipitated with the 2C1 anti-ATM antibody. Kinase reactions (*top*) were performed in the presence of purified GST-tagged TET1, GST-tagged TET1^{S116A} and GST-tagged TET1$^{S116A/S262A/S546A}$

(continued)

Manipulation of TET1 activity affects DNA damage signalling

TET1-mediated conversion of 5mC to 5hmC in DNA damage response suggests that TET1 activity plays a role in DNA damage signalling. To address this, GFP, GFP-TET1 and GFP-Cas9-Tet1 were transfected into log phase neuronal N2a cells. The levels and numbers of γ-H2AX foci decreased within 6 h of etoposide treatment in GFP-TET1-expressing cells in contrast to GFP-expressing cells (Fig. 4A and B). Western blots confirmed that overexpression of TET1 led to quicker extinction of γ-H2AX and ^{P}S15-p53 in DNA damage response (Fig. 4C and D). A similar result was found in HT22 cells (Supplementary Fig. 4). Nevertheless, an increased intensity of γ-H2AX foci and the elevated γ-H2AX and ^{P}S15-p53 were found in GFP-Cas9-Tet1-expressing cells, suggesting that TET1 increases speed of recovery, but Cas9-Tet1 seems to attenuate DNA repair (Fig. 4A and B). This implies that TET1 regulates DNA damage signalling and that the level of 5hmC may be an important quantitative factor in the pace of DNA repair.

Knockdown of TET1 induces cell cycle re-entry and neuronal death

Our earlier studies demonstrated that ATM deficiency directly leads to neuronal cell cycle re-entry and defective DNA damage response (Yang and Herrup, 2005; Li *et al.*, 2012, 2013). We therefore asked whether TET1-mediated conversion of 5mC to 5hmC was involved in the ability of ATM to regulate the neuronal cell cycle. Primary neurons from wild-type and *Atm*$^{-/-}$ mice embryonic cortex were infected with lentiviral shRNAs against *Tet1*, *Tet2* and *Tet3* at *in vitro* Day 5. Neurons were treated with 10 Gy γ-irradiation and fixed with 4% paraformaldehyde at *in vitro* Day 7. Knockdown of TET1 significantly increased bromodeoxyuridine incorporation (Fig. 5A and B), and also promoted γ-irradiation-induced activation of caspase 3 in both wild-type and *Atm*$^{-/-}$ primary neurons (Fig. 5C and D). However, there was little effect with either *Tet2* or *Tet3* shRNAs (*shTet2* or *shTet3*) infection (Fig. 5E–H). These data suggested that TET1, but not TET2 or TET3, is likely involved in ATM-dependent DNA damage signalling as well as neuronal cell cycle re-entry in ATM deficiency.

Hydroxymethylated DNA immunoprecipitation sequencing indicates a region-specific genome-wide shift in 5hmC marking

To identify genomic regions affected by the selective loss of 5hmC in ATM deficiency, we performed hydroxymethylated DNA immunoprecipitation sequencing (hMeDIP-seq). While the distribution of aligned sequences across the genome was similar (Supplementary Fig. 5), a large proportion of aligned sequences was found to overlap repeated genomic elements, as defined by the RepeatMasker track from the UCSC genome browser (Fig. 6A), and both the levels of 5mC and 5hmC in gene loci at transcription start sites showed differential alteration in ataxia-telangiectasia (Supplementary Fig. 6). There is a clear decrease in overlap with long terminal repeats when comparing control cerebellar cortex samples to input DNA ($P = 0.007$, ANOVA), and a trend toward an increase in SINE alignments ($P = 0.058$, ANOVA), similar to previous results (Szulwach *et al.*, 2011*b*). However, there were no differences found in similar preparations from cortex (Supplementary Fig. 5). Furthermore, the fraction of SINE alignments increases in cerebellar cortex from ataxia-telangiectasia patients ($P = 0.0002$) at the expense of a decrease in unique, non-repeated sequence alignments ($P = 0.001$), and this is also not observed in cortex. Similar results were identified in 5hmC hMeDIP-seq from FACS-isolated mouse Purkinje cell (Supplementary Fig. 7A–C). These shifts in alignment patterns are evidence of a tissue-specific, genome-wide shift in 5hmC marking in ataxia-telangiectasia.

Next, we focused on the methyl-enriched regions of CpG islands by selecting the subset of immunoprecipitation-enriched genome intervals overlapping the CpG track from the UCSC genome browser. The Venn diagram in Fig. 2C shows that of the 24 324 genomic intervals that satisfied at least one of these conditions, 6543 genome elements (~27%) satisfied both (Fig. 6B). A much smaller number of 5hmC marks were found to be different between control and ataxia-telangiectasia cortex and the overlap between cortical and cerebellar marks was small as well. The gene ontology (GO) biological functions suggested that 5hmC loss could affect a number of classes of neuron-specific functions, particularly markers of differentiation (Fig. 6C).

Figure 2 Continued

(3SA) (1 μg of each) as indicated. Coomassie blue staining (*bottom*) was used to demonstrate total protein load. (**F**) GFP-TET1 and Flag-ATM were transfected into *Atm*$^{-/-}$ mouse embryonic fibroblasts. Lysates were immunoprecipitated with anti-GFP antibody and blotted with ^{P}[S/T]Q antibody plus anti-GFP and anti-Flag. Flag antibody was used for the quality control of Flag-ATM-WT and KD expression. (**G**) 5hmC-specific dot-blot intensities of genomic DNA isolated from *Atm*$^{-/-}$ mouse embryonic fibroblasts with overexpression of GFP-TET1-WT, 3SA with Flag-ATM. (**H**) Quantification of three repetitions of the experiment illustrated in **G**. Amounts of 5hmC are shown as a percentage of total genomic DNA (*$P < 0.05$, Student's *t*-test; mean ± SEM). IB = immunoblot; IP = immunoprecipitation; NT = no treatment; IR = γ-irradiation.

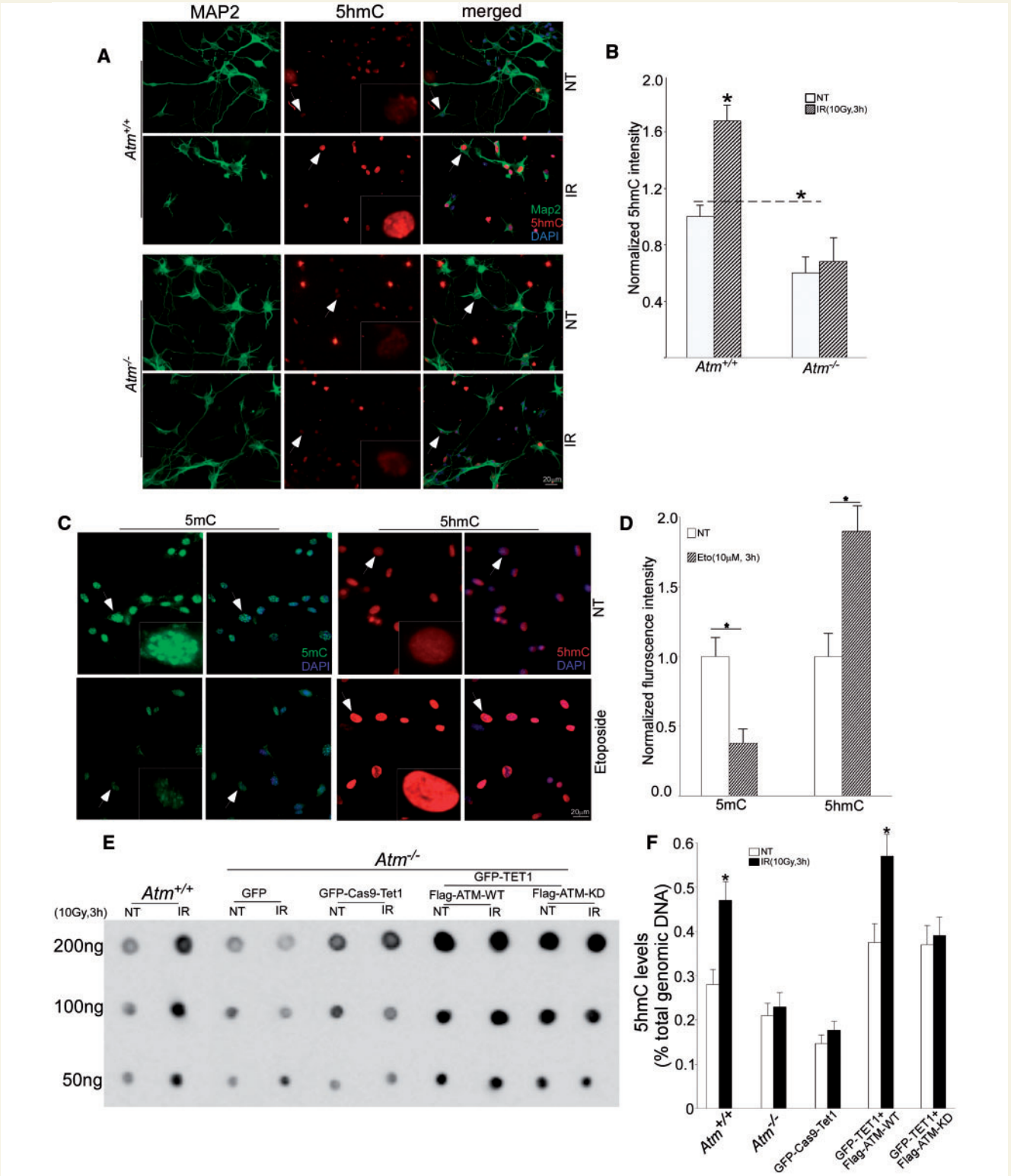

Figure 3 TET1-mediated 5hmC production responds to ATM-dependent DNA damage. (**A**) *In vitro* Day 10 embryonic Day 16.5 neuronal cultures from wild-type ($Atm^{+/+}$) and $Atm^{-/-}$ embryos were stained with 5hmC (red, white arrows) and MAP2 (green) after γ-irradiation treatment. (**B**) Quantification of intensities of 5hmC such as those illustrated in **A**. Each bar represents the average of three independent experiments. Data are presented as mean ± SEM. (n = 36–88 cells). *$P < 0.001$. (**C**) HT22 cells were stained with 5hmC and 5mC after etoposide treatment. (**D**) Quantification of intensities of 5hmC and 5mC such as those illustrated in **C**. Each bar represents the average of three independent experiments. Data are presented as mean ± SEM. (n = 316–550 cells). *$P < 0.001$. (**E**) 5hmC-specific dot-blot intensities of genomic DNA isolated from $Atm^{-/-}$ mouse embryonic fibroblasts with overexpression of GFP-Cas9-Tet1, GFP-TET1 with Flag-ATM. (**F**) Quantification of three repetitions of the experiment illustrated in **E**. Amounts of 5hmC are shown as a percentage of total genomic DNA (*$P < 0.05$, Student's t-test; mean ± SEM).

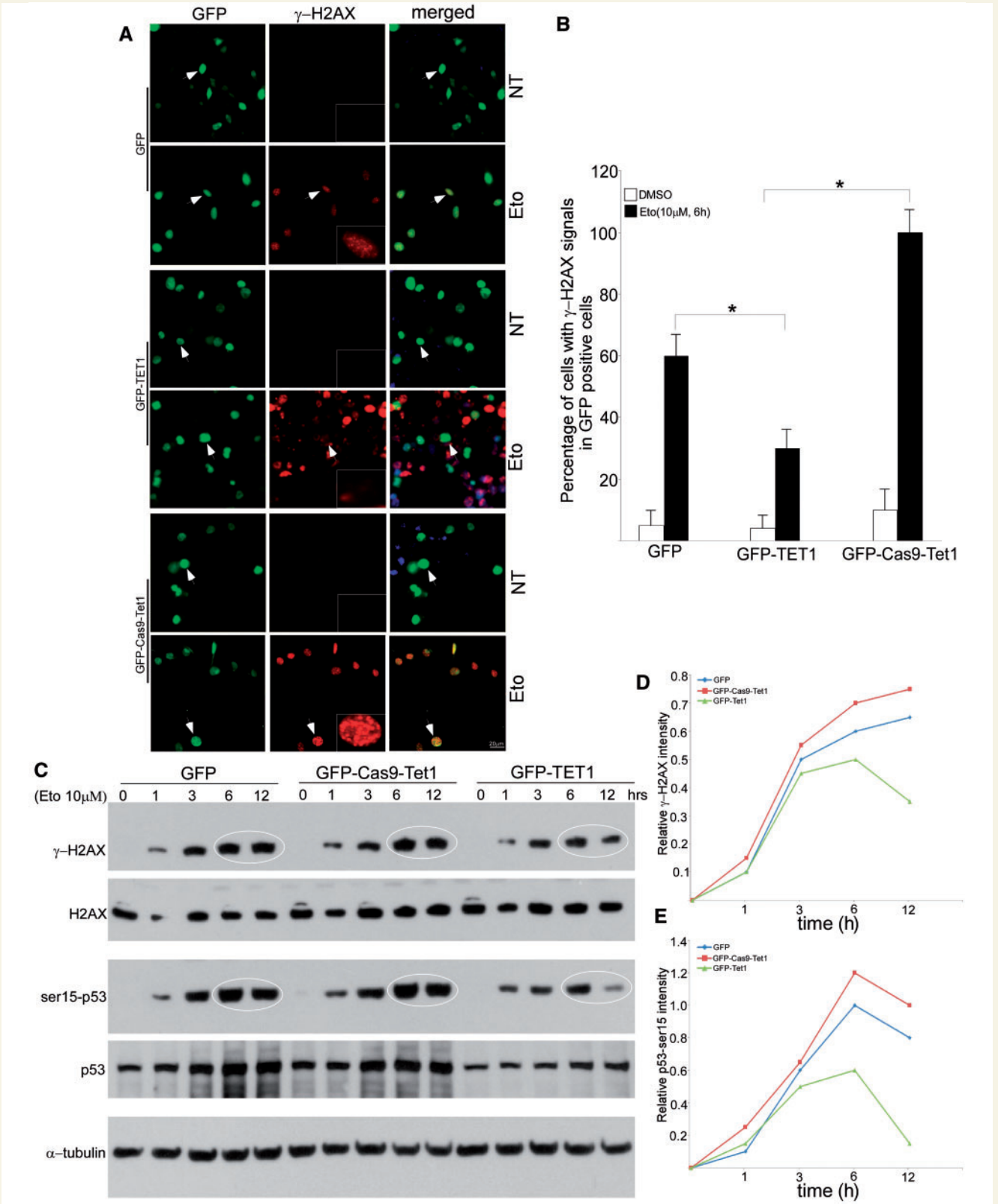

Figure 4 TET1 regulates the DNA damage response. (**A**) N2a cells were transfected with GFP, GFP-Cas9-Tet1 and GFP-TET1. 2 days later, cells were treated with etoposide for 6 h, then fixed and stained with γ-H2AX (white arrows) antibody. The white circles indicate positive cells. (**B**) The relative intensity and number of γ-H2AX foci immunostaining illustrated in **A**. Data are presented as mean ± SEM. (n = 120–186 cells). *$P < 0.05$. (**C**) Protein extracts from GFP-, GFP-Cas9-Tet1- or GFP-TET1-expressing N2a cells with or without etoposide treatment was analysed by western blot. DMSO = dimethyl sulphoxide.

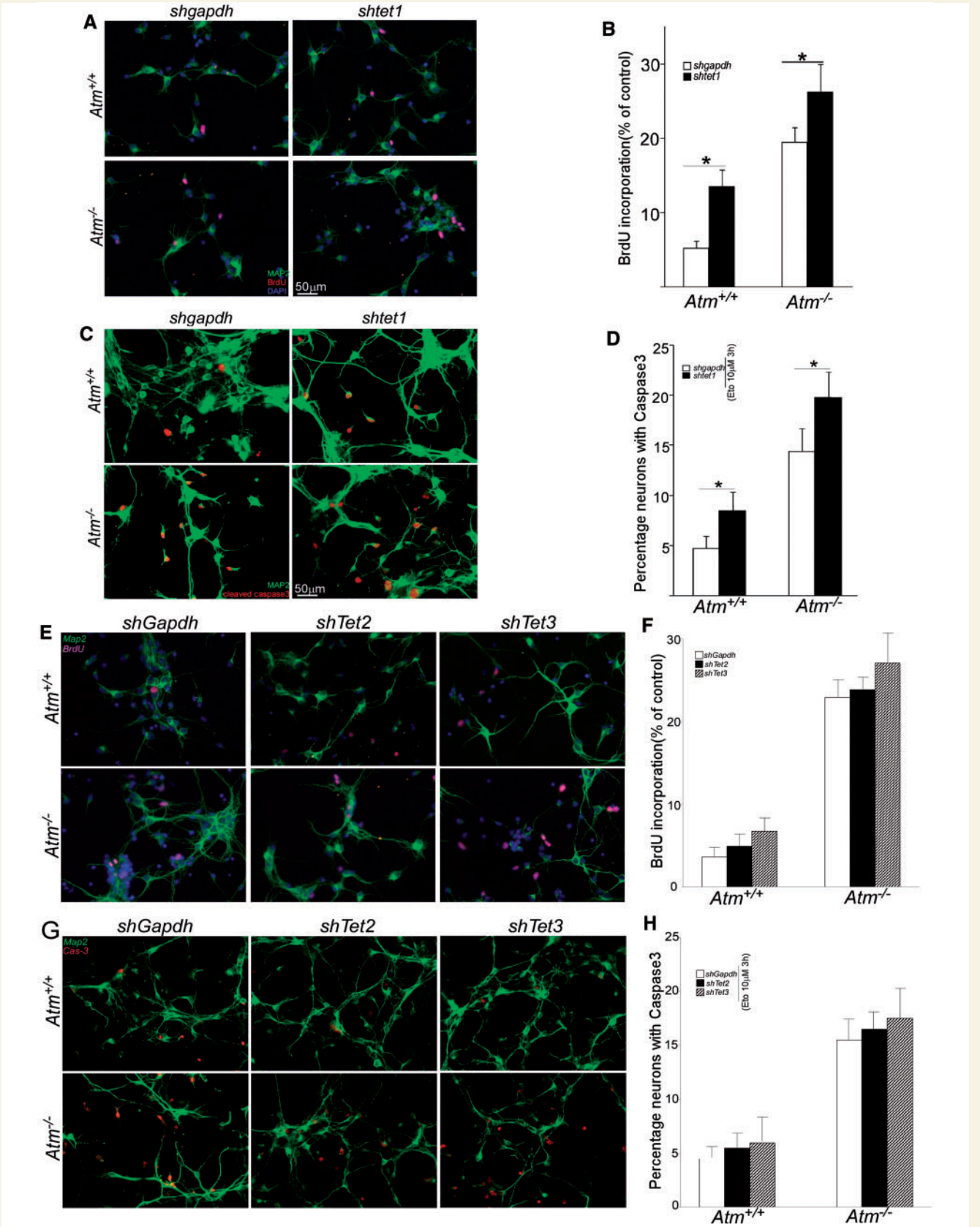

Figure 5 TET1 regulates neuronal health and survival in ATM deficiency. (**A** and **B**) Embryonic Day 16.5 cortical neurons were infected at *in vitro* Day 3 with either *shGapdh* or *shTet1* lentiviral particles. MAP2/BrdU double-labelled cells numbers are displayed as a per cent of the total number of MAP2-positive cells. Data are presented as mean ± SEM (n = 66–89 cells). *$P < 0.05$. (**C** and **D**) Embryonic Day 16.5 cortical neurons were infected at *in vitro* Day 3 with either *shGapdh* or *shTet1* lentiviral particles. Cell death was quantified by counting the number of

(continued)

Starting with Illumina microarray gene expression data comparing human cerebellar samples from ataxia-telangiectasia ($n = 3$) and controls ($n = 4$), we examined the distribution of the fold-change ratio for the genes in both the 5mC, 5hmC or overlapping selected sets. The results show a general decrease in the relative expression in ataxia-telangiectasia (each is significantly reduced compared with all genes, ANOVA, $P < 0.001$, Fig. 6D), as would be predicted as DNA methylation tends to reduce gene expression. For the genes in the overlapping set, the positioning of detected 5hmC marks was distinctly different between cortex and cerebellum (Fig. 6E). A small but clear increase in 5hmC-marked gene body sequences was also observed in ataxia-telangiectasia. We also identified the subset from the overlapping set of genes where the decrease in expression is substantial and significant [with the absolute value of the $\log_2$ fold-change > 1 and the false discovery rate (FDR) < 0.05; Fig. 6F]. Predicted functions include development, particularly nervous system development, and one of the three significant upstream regulators is ATM (Supplementary Fig. 8). The most prominent networks enriched in these analyses, nervous system development and neurological diseases, are depicted in Supplementary Fig. 8. Thus, this study establishes the first comparative genome-wide map of the hydroxylmethylome in control and ataxia-telangiectasia cerebellum and reveals a region-specific shift of 5hmC from the epigenome of neurons in the ataxia-telangiectasia brain.

To assess the direct effect of decreased enrichment of 5hmC in the promoter regions of Purkinje cell-specific genes including *Pcp2*, *En1*, *Hsph1* and *Cbln1*, we examined protein levels and mRNA expression in wild-type and $Atm^{-/-}$ cerebella. Consistent with the 5hmC-seq data, we found a significant reduction of gene expression in $Atm^{-/-}$samples (Supplementary Fig. 9).

Manipulation of TET1 activity affects Purkinje cell vulnerability and behavioural deficits in $Atm^{-/-}$ mice

Earlier studies demonstrated Purkinje cell anomalies and behavioural deficits in $Atm^{-/-}$ mice (Barlow *et al.*, 1996; Kuljis *et al.*, 1997; Li *et al.*, 2012, 2013). We therefore sought to determine whether TET1-mediated conversion of 5mC to 5hmC was involved in the Purkinje cell vulnerability as well as in the behavioural deficits observed in $Atm^{-/-}$ mice. To address this, adenoviral particles encoding human wild-type TET1 (AAV TET1-WT) and kinase dead mutant (AAV TET1-KD) were co-infected with lentiviral shRNA particles specifically against mouse *Tet1* into the wild-type and $Atm^{-/-}$ mice cerebellar slice cultures. Two weeks after viral infection, gene transfer was monitored by TET1 staining (Supplementary Fig. 10A). Cleaved caspase 3, a cell death marker, was used to determine the effect of TET1 on the degenerative process of Purkinje cells. In cerebellar Purkinje cells with knockdown of TET1, overexpression of TET1-WT prevented activation of caspase 3 in Purkinje cells. However, overexpression of TET1-KD had little effect on activation of caspase 3 in either wild-type or $Atm^{-/-}$ Purkinje cells (Supplementary Fig. 10B and C). To further define this finding *in vivo*, adenoviral particles encoding human wild-type TET1 (AAV TET1-WT) and kinase dead mutant (AAV TET1-KD) were co-injected with lentiviral shRNA particles specifically against mouse *Tet1* into the wild-type and $Atm^{-/-}$ mice cerebellum. Three weeks after viral injection, cleaved caspase 3 immunostaining was used to assess the effect of TET1 on the degenerative process in the Purkinje cells. In control infected wild-type Purkinje cells (*shGapdh* only), there was no evident appearance of caspase 3 staining; similarly, in control infected $Atm^{-/-}$ Purkinje cells there was no decrease observed in the already elevated baseline caspase 3 activation. Reduction of endogenous mouse TET1 by *shTet1* led to an increase in caspase 3 activation (Fig. 5 and data not shown). Simultaneous overexpression of TET1-WT, however, prevented this increase in Purkinje cells (Fig. 7A and B). This is a TET1-specific effect as shown by the fact that overexpression of TET1-KD failed to increase 5hmC and had little effect on activation of caspase 3 in either wild-type or $Atm^{-/-}$ Purkinje cells (Fig. 7A and B).

We tested the consequences of these changes on the role of TET1 in the context of the whole animal by examining the reduced motor coordination of $Atm^{-/-}$ mice compared to wild-type mice. We co-injected *shTet1*-encoding lentiviral particles along with wild-type (AAV-TET1-WT) and kinase dead (AAV-TET1-KD) TET1 encoding adenoviral particles. The injections were targeted at mouse cerebellum at postnatal Day 18—an age at which the areas reached by viral infection should be greater than in the adult. Three weeks after intracerebellar infusions, we subjected animals to rotarod testing and measured locomotor activity in an open field. In the rotarod test, the *shTet1* and AAV-TET1-WT co-injected $Atm^{-/-}$ mice showed a significant delay in falling ($P = 0.0013$) compared to $Atm^{-/-}$ mutants infused with *shTet1* and AAV-TET1-KD (Fig. 7C). Furthermore,

Figure 5 Continued

activated caspase 3 immunostained cells as a percentage of the total DAPI-stained nuclear counts. Data are presented as mean ± SEM ($n = 42$–81 cells), $^*P < 0.05$. (**E** and **F**) Embryonic Day 16.5 cortical neurons were infected at *in vitro* Day 3 with either *shGapdh* or *shTet2* and *shTet3* lentiviral particles. MAP2/BrdU double-labelled cells numbers are displayed as per cent of the total number of MAP2-positive cells. Data are presented as mean ± SEM ($n = 53$–101 cells), $^*P < 0.05$. (**G** and **H**) Embryonic Day 16.5 cortical neurons were infected at *in vitro* Day 3 with either *shGapdh* or *shTet2* and *shTet3* lentiviral particles. Cell death was quantified by counting the number of activated caspase 3 immunostained cells as a percentage of the total DAPI-stained nuclear counts. Data are presented as mean ± SEM ($n = 72$–109 cells), $^*P < 0.05$.

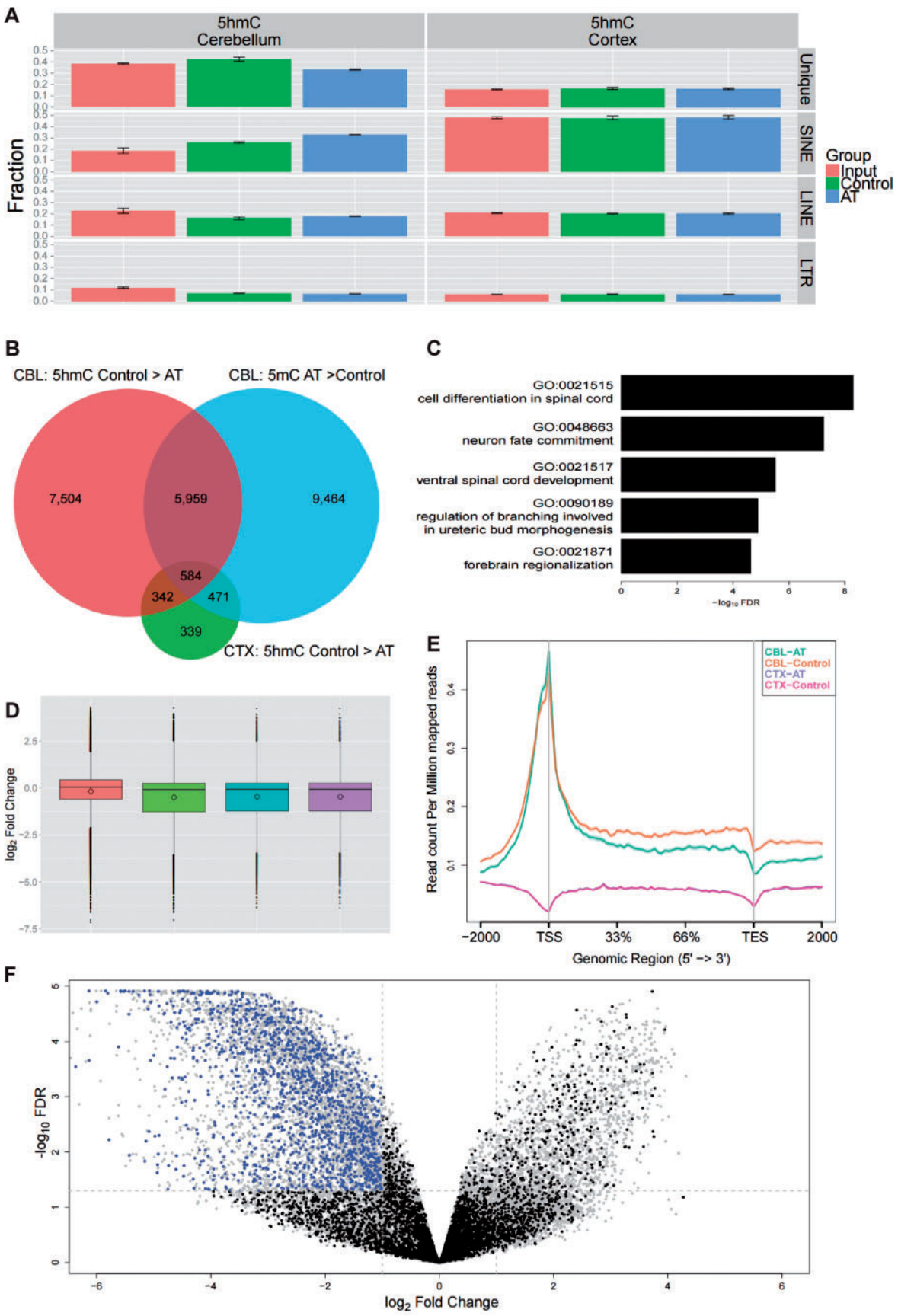

Figure 6 Methyl-nucleotide immunoprecipitation-sequencing (MeDIP-seq) identifies genes predicted to be dysregulated by loss of ATM function. (**A**) Sequencing reads of DNA fragments immunoprecipitated with anti-5hmC were enriched in repeated genome

(continued)

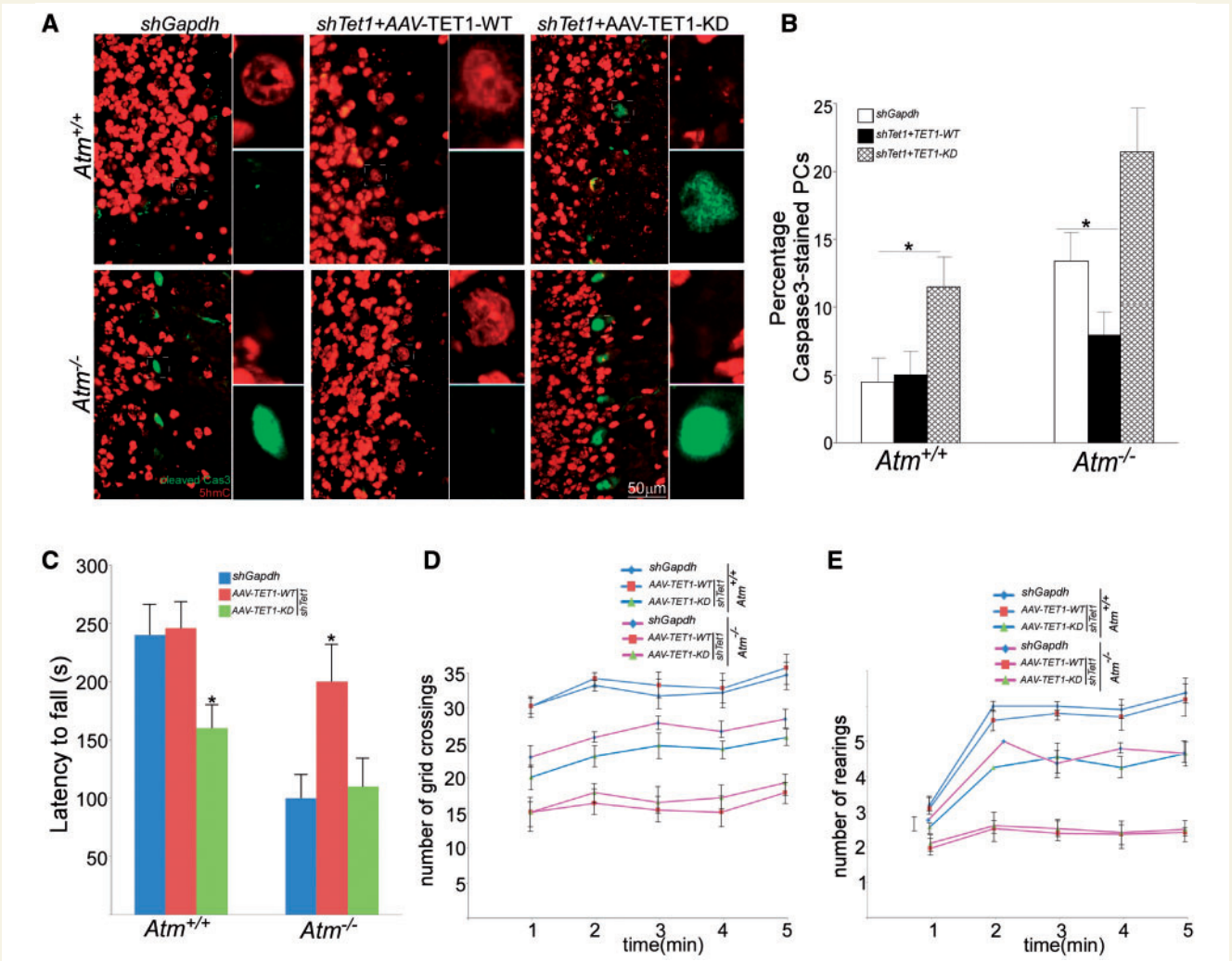

Figure 7 TET1 activity links to Purkinje cell degeneration and behavioural deficits in *Atm*$^{-/-}$ mice. (**A**) Representative images of cleaved caspase3- (green) and 5hmC- (red) stained Purkinje cells show the effects of TET1 activity on Purkinje cell vulnerability. Scale bar = 50 μM. (**B**) Quantification of the cleaved caspase 3-stained Purkinje cells was shown in **A**. Each bar represents the average of three independent experiments. Error bars represents standard deviation between slides. Five to seven images per slide, six slides per mouse. Data are presented as mean ± SEM, ***$P < 0.001$, one-way ANOVA. (**C**) Rota-rod testing demonstrated that *shTet1* and AAV-TET1-WT coinjected *Atm*$^{-/-}$ mice had longer latency-to-fall times. Time measured to remain on the rota-rod was analysed by a two-way ANOVA and found to reveal a significant genotype × treatment interaction [$F(2,45) = 20.1$, *$P < 0.0001$]. (**D** and **E**) Locomotor activity and rearing in the open field were measured across 1-min bins for a total of five consecutive minutes. For distance travelled, a two-way ANOVA with repeated measures revealed significant effects of genotype [$F(1,45) = 35.8$, $P < 0.0001$] and treatment [$F(2,45) = 3.8$, $P < 0.026$] and a genotype × treatment interaction [$F(2,45) = 3.4$, $P < 0.05$]. The latter was supported by a clear separation of values in *Atm*$^{-/-}$ mice between those given AAV-TET1-WT and KD as well as and those administered *shGapdh;* for rearing, significant main effects [group: $F(1,45) = 161.9$, $P < 0.0001$; treatment: $F(2,45) = 24.0$, $P < 0.0001$] and an interaction [$F(2,45) = 12.7$, $P < 0.0001$] were similarly observed.

Figure 6 Continued

regions. (**B**) A Venn diagram showing the numbers and overlap of genomic intervals satisfying the hypothesis of having nearby CpG islands marked by enriched 5mC in ataxia-telangiectasia (blue circle) and enriched 5hmC marks in Control (reduced in ataxia-telangiectasia; red circle). (**C**) The top five GO terms enriched in the intersected reduced 5hmC and enriched 5mC regions in ataxia-telangiectasia, as determined by GREAT, plotting the $-\log_{10}$ of the false discovery rate (FDR; *P*-value corrected for multiple measurements). (**D**) Relative gene expression analysis of groups of genes marked with enriched 5mC in ataxia-telangiectasia (green), reduced 5hmC in ataxia-telangiectasia (blue), or the intersect set (violet) compared with all genes (red). All three selected groups of genes exhibit a significantly different mean ratio of gene expression than all genes ($P < 0.001$, ANOVA). (**E**) Alignment of sequencing reads across the summed genomic region shows increased marking of the transcription start site (TSS) region in cerebellum compared with cortex (CTX-control overlaps and partially obscures CTX-AT) as well as an ataxia-telangiectasia specific increase in marks in the gene body. (**F**) The intersecting set of gene expression profiles is displayed as a volcano plot (black dots). Genes were selected for functional analysis based on having a $\log_2$ fold change ⩽ 1 and a FDR ⩽ 5% (blue dots). CBL = cerebellar cortex; CTX = cerebral cortex.

spontaneous open field activity (measured as distance travelled) was significantly greater in *shTet1* and AAV-TET1-WT co-injection, approaching wild-type values (Fig. 7D). A secondary parameter of ataxic behaviour, rearing, was also different dependent on genotype and treatment. Wild-type mice reared more often ($P = 0.023$) than mutants receiving virus encoding *shGapdh* (Fig. 7E). However, *shTet1* and AAV-TET1-KD co-injected $Atm^{-/-}$ mice showed a reversal of the deficiency (Fig. 7C–E). These results indicate that TET1-mediated production of 5hmC links to ATM-deficient Purkinje cell degeneration as well as the ataxia-telangiectasia neurological symptoms that are expressed in the Atm^{tm1Bal} mouse model.

Discussion

ATM is ubiquitously expressed throughout the body and is found in a wide variety of cells located in regions throughout the brain. While ATM is best known for its role in the DNA damage response, it is increasingly clear that defects in the DNA damage response alone cannot fully account for the range of neurological and neuropathological changes that are observed in patients with ataxia-telangiectasia. Finding the mechanisms behind the neurodegeneration in ATM deficiency is thus crucial for understanding the mechanism of ataxia-telangiectasia neurological symptoms. One of the most difficult challenges in this search is to explain in molecular terms how a genetic change that is found in the nucleus of every cell in the brain can somehow selectively promote Purkinje cell vulnerability. Here we present multiple lines of evidence supporting an important role for abnormalities in the DNA demethylation enzyme, TET1, and the resulting changes in DNA hydroxymethylation in the generation of this cell type specificity.

The recent discovery of the role of the TET family in the control of genomic DNA modifications has opened a new and potentially valuable window into the regulation of gene expression in health and in disease. While all three TET family members catalyse the conversion of 5mC to 5hmC, each TET-dependent 5hmC production shows distinct regulation in different brain functions (West, 2015; Yu *et al.*, 2015). It is also increasingly evident that 5hmC is not simply an intermediate in the demethylation reaction; rather this newly discovered DNA modification has its own role to play in the regulation of chromatin dynamics and gene expression. It is in this context that our observations of a TET1-dependent regulation of 5hmC levels and its sensitivity to regulation by ATM gain considerable significance. Acting through the action of ATM the suggestion is that these alterations in DNA hydroxymethylation are closely tied to the neuronal DNA damage response and affect the timing and perhaps other features of its outcome. Chromatin status is well known to impact the process of DNA damage signalling and repair. The involvement of ATM, acting through TET1-mediated 5hmC production, implies that chromatin structure is itself altered as part of the repair process. Further, the results in Fig. 4 imply that this alteration, perhaps in conjunction with changes in histone methylation (Li *et al.*, 2012), is required to achieve normal repair kinetics. This scenario is consistent with prior reports that ATM-dependent phosphorylation of KAP1 (encoded by *TRIM28*), a heterochromatin formation factor, is involved in the slower kinetics of DNA repair in or near areas of heterochromatin (Goodarzi *et al.*, 2010). Therefore, just as ATM acts in multiple independent ways to regulate the histone code, the same may be true for its effects on the regulation of DNA demethylation. This suggests that TET1-mediated active DNA demethylation during the ATM-dependent DNA damage response contributes to DNA double-strand break repair. Interestingly, preliminary findings in our laboratory indicate that TET3-dependent 5hmC production is sensitive to ATR-mediate single strand DNA breaks. In future work, thus, it will be worth assessing what role each TET isoform plays in response to different types of DNA damage.

The abundance of all three TET proteins as well as 5hmC in animal and human brains further suggests important roles of TET-dependent 5hmC production in neuronal health and survival (Xu *et al.*, 2011). This raises the question of the normal role of TET1 and 5hmC in the physiology of the neuron. Immunocytochemistry suggests that 5hmC is found in many cell types, including Purkinje cells. Yet compared to Purkinje cells the density of 5hmC staining is much greater in cerebellar and hippocampal granule cells as well as in cortical neurons (Fig. 1 and Supplementary Fig. 1). It seems almost paradoxical, therefore, that in human ataxia-telangiectasia and $Atm^{-/-}$ mouse models, there is a significant loss of 5hmC in Purkinje neurons but not in other neuronal types. Perhaps it is precisely because the levels are low that loss of ATM-dependent TET1 activity and the consequent decline in Purkinje cell 5hmC levels are so detrimental to the cell.

HMeDIP-seq data reveal a significant genome-wide shift in the 5hmC landscape in ataxia-telangiectasia cerebellar cortex but not in samples of frontal cortex. This is particularly noteworthy as it can be assessed by the proportion of sequencing reads overlapping repeated elements in the genome, a direct measure that is independent of algorithms to identify enriched regions, for example. These changes in 5hmC marks, while widely distributed across the genome, do not appear to be random. Our comparison of the 5hmC and 5mC DIP-seq data in conjunction with the immunocytochemistry is revealing. It suggests that when TET1 activity is reduced (as in ATM deficiency), not only is 5hmC-mediated regulation of gene expression compromised, there is also a dysregulation of 5mC-dependent epigenetic system. In tabulating the 'ontology' of the genes whose 5hmC levels fall at the same time as their 5mC levels rise, we find it noteworthy that many genes whose function is critical for cerebellar development are identified. The suggestion is that ATM regulation of 5hmC-dependent epigenetic system may also influence developmental

functions such as fate specification and perhaps maintain these properties in mature cells.

Our hMeDIP-seq analysis shows a high correlation between 5hmC enrichments and dysregulation of neuronal differentiation-specific functional genes found in ATM deficiency. One potential role for such alterations in TET1-mediated 5hmC enrichment is the cell type specificity observed when ATM is deficient. Overexpression of wild-type TET1 but not a kinase mutant not only increases 5hmC level but also prevents Purkinje cell degeneration and improves the behavioural deficits found in $Atm^{-/-}$ mice.

As the most prominently affected cells in the ataxia-telangiectasia brain are the cerebellar Purkinje cells, we propose that the loss of 5hmC caused by ATM deficiency may help to explain their unique vulnerability. Alterations in the levels of 5hmC occur in other neuronal cell subtypes in ataxia-telangiectasia, but the baseline of 5hmC in Purkinje cells appears relatively low. The suggestion is that the margin of error may be much smaller for Purkinje cells than for other cells types and so in ataxia-telangiectasia, they are the first and most prominent 'victims' of the 5hmC deficiency. We would further predict that this vulnerability may be time and region-specific and that non-genetic factors that reduced ATM function in other situations could lead to the loss of other neuronal cell types. This idea receives some support from our recent preliminary data derived from the study of human Alzheimer's disease brain, in which the selective loss of 5hmC are found in the degenerative neurons in human Alzheimer's disease prefrontal cortex and hippocampus. Together with the behavioural data (Fig. 7), the suggestion is that dysregulation of the 5hmC-mediated epigenetic system may not be the trigger; however, it could play a decisive role in driving cell type-specific neurodegeneration. If this relationship proves true, it suggests that would be value in investigating changes in 5hmC during the pathogenesis of other neurodegenerative disorders. If our hypothesis is correct, it might reveal that determining the epigenetic signatures in different cell populations would aid in differential diagnosis of disease and may offer a pathway to the discovery of novel therapeutic targets.

Acknowledgements

We thank Dr Richard Gatti (UCLA, Los Angles) for sharing human A-T paraffin-fixed samples. We thank Dr Yang Xu (UCSD, San Diego) for providing Atm^{tmlBal} mutant strain. Human frozen tissue was obtained from NICHD Brain and Tissue Bank of Developmental Disorders at the University of Maryland, Baltimore, MD. We thank Dr Heinrich Leonhardt (Ludwig Maximilians University Munich) for providing the GFP-TET1 plasmids.

Funding

This work was supported by the Chinese Academy of Sciences (Y406541141 and 1100050210) to J.L. and the National Science Foundation of China (NSFC 81471313) to J.L. as well as the National Key Basic Research Program of China (2015CB755600). The support of the A-T Children's Project to K.H. and R.P.H. is gratefully acknowledged. This work was also supported by grants from the NIH (NS20591 and NS71022) and the National Key Basic Research Program of China (2013CB530900) as well as The Hong Kong University of Science and Technology and the Hong Kong Research Grants Council, HKSAR (GRF660813) to K.H. NIH support was also provided (R21 DA032984) to R.P.H.

Supplementary material

Supplementary material is available at *Brain* online.

References

Barlow C, Hirotsune S, Paylor R, Liyanage M, Eckhaus M, Collins F, et al. Atm-deficient mice: a paradigm of ataxia telangiectasia. Cell 1996; 86: 159–71.

Chakrabarti L, Zahra R, Jackson SM, Kazemi-Esfarjani P, Sopher BL, Mason AG, et al. Mitochondrial dysfunction in nnad mutant flies and purkinje cell degeneration mice reveals a role for nna proteins in neuronal bioenergetics. Neuron 2010; 66: 835–47.

Chaudhry MA, Omaruddin RA. Differential DNA methylation alterations in radiation-sensitive and -resistant cells. DNA Cell Biol 2012; 31: 908–16.

Chia N, Wang L, Lu X, Senut MC, Brenner C, Ruden DM. Hypothesis: environmental regulation of 5-hydroxymethylcytosine by oxidative stress. Epigenetics 2011; 6: 853–6.

Deaton AM, Bird A. Cpg islands and the regulation of transcription. Genes Dev 2011; 25: 1010–22.

Feng J, Liu T, Qin B, Zhang Y, Liu XS. Identifying chip-seq enrichment using macs. Nat Protoc 2012; 7: 1728–40.

Globisch D, Munzel M, Muller M, Michalakis S, Wagner M, Koch S, et al. Tissue distribution of 5-hydroxymethylcytosine and search for active demethylation intermediates. PLoS One 2010; 5: e15367.

Goodarzi AA, Jeggo P, Lobrich M. The influence of heterochromatin on DNA double strand break repair: getting the strong, silent type to relax. DNA Repair (Amst) 2010; 9: 1273–82.

Guo JU, Su Y, Zhong C, Ming GL, Song H. Hydroxylation of 5-methylcytosine by tet1 promotes active DNA demethylation in the adult brain. Cell 2011; 145: 423–34.

Haffner MC, Chaux A, Meeker AK, Esopi DM, Gerber J, Pellakuru LG, et al. Global 5-hydroxymethylcytosine content is significantly reduced in tissue stem/progenitor cell compartments and in human cancers. Oncotarget 2011; 2: 627–37.

He YF, Li BZ, Li Z, Liu P, Wang Y, Tang Q, et al. Tet-mediated formation of 5-carboxylcytosine and its excision by tdg in mammalian DNA. Science 2011; 333: 1303–7.

Ito S, D'Alessio AC, Taranova OV, Hong K, Sowers LC, Zhang Y. Role of tet proteins in 5mc to 5hmc conversion, es-cell self-renewal and inner cell mass specification. Nature 2010; 466: 1129–33.

Ito S, Shen L, Dai Q, Wu SC, Collins LB, Swenberg JA, et al. Tet proteins can convert 5-methylcytosine to 5-formylcytosine and 5-carboxylcytosine. Science 2011; 333: 1300–3.

Jin SG, Wu X, Li AX, Pfeifer GP. Genomic mapping of 5-hydroxymethylcytosine in the human brain. Nucleic Acids Res 2011; 39: 5015–24.

Kraus TF, Globisch D, Wagner M, Eigenbrod S, Widmann D, Munzel M, et al. Low values of 5-hydroxymethylcytosine (5hmc), the "sixth base," are associated with anaplasia in human brain tumors. Int J Cancer 2012; 131: 1577–90.

Kriaucionis S, Heintz N. The nuclear DNA base 5-hydroxymethylcytosine is present in purkinje neurons and the brain. Science 2009; 324: 929–30.

Kudo Y, Tateishi K, Yamamoto K, Yamamoto S, Asaoka Y, Ijichi H, et al. Loss of 5-hydroxymethylcytosine is accompanied with malignant cellular transformation. Cancer Sci 2012; 103: 670–6.

Kuljis RO, Xu Y, Aguila MC, Baltimore D. Degeneration of neurons, synapses, and neuropil and glial activation in a murine atm knockout model of ataxia-telangiectasia. Proc Natl Acad Sci U S A 1997; 94: 12688–93.

Langmead B, Trapnell C, Pop M, Salzberg SL. Ultrafast and memory-efficient alignment of short DNA sequences to the human genome. Genome Biol 2009; 10: R25.

Li J, Chen J, Ricupero CL, Hart RP, Schwartz MS, Kusnecov A, et al. Nuclear accumulation of hdac4 in atm deficiency promotes neurodegeneration in ataxia telangiectasia. Nat Med 2012; 18: 783–90.

Li J, Chen J, Vinters HV, Gatti RA, Herrup K. Stable brain atm message and residual kinase-active atm protein in ataxia-telangiectasia. J Neurosci 2011; 31: 7568–77.

Li J, Hart RP, Mallimo EM, Swerdel MR, Kusnecov AW, Herrup K. Ezh2-mediated h3k27 trimethylation mediates neurodegeneration in ataxia-telangiectasia. Nat Neurosci 2013; 16: 1745–53.

Li W, Liu M. Distribution of 5-hydroxymethylcytosine in different human tissues. J Nucleic Acids 2011; 2011: 870726.

Lian CG, Xu Y, Ceol C, Wu F, Larson A, Dresser K, et al. Loss of 5-hydroxymethylcytosine is an epigenetic hallmark of melanoma. Cell 2012; 150: 1135–46.

Malzkorn B, Wolter M, Riemenschneider MJ, Reifenberger G. Unraveling the glioma epigenome: from molecular mechanisms to novel biomarkers and therapeutic targets. Brain Pathol 2011; 21: 619–32.

Pastor WA, Pape UJ, Huang Y, Henderson HR, Lister R, Ko M, et al. Genome-wide mapping of 5-hydroxymethylcytosine in embryonic stem cells. Nature 2011; 473: 394–7.

Quinlan AR, Hall IM. Bedtools: a flexible suite of utilities for comparing genomic features. Bioinformatics 2010; 26: 841–2.

Shen L, Shao N, Liu X, Nestler E. Ngs.Plot: quick mining and visualization of next-generation sequencing data by integrating genomic databases. BMC Genomics 2014; 15: 284.

Smyth GK Limma: linear models for microarray data. Bioinformatics and computational biology solutions using r and bioconductor. New York: Springer; 2005. p. 397–420.

Song CX, Szulwach KE, Fu Y, Dai Q, Yi C, Li X, et al. Selective chemical labeling reveals the genome-wide distribution of 5-hydroxymethylcytosine. Nat Biotechnol 2011; 29: 68–72.

Szulwach KE, Li X, Li Y, Song CX, Han JW, Kim S, et al. Integrating 5-hydroxymethylcytosine into the epigenomic landscape of human embryonic stem cells. PLoS Genet 2011a; 7: e1002154.

Szulwach KE, Li X, Li Y, Song CX, Wu H, Dai Q, et al. 5-hmc-mediated epigenetic dynamics during postnatal neurodevelopment and aging. Nat Neurosci 2011b; 14: 1607–16.

Szwagierczak A, Bultmann S, Schmidt CS, Spada F, Leonhardt H. Sensitive enzymatic quantification of 5-hydroxymethylcytosine in genomic DNA. Nucleic Acids Res 2010; 38: e181.

Tahiliani M, Koh KP, Shen Y, Pastor WA, Bandukwala H, Brudno Y, et al. Conversion of 5-methylcytosine to 5-hydroxymethylcytosine in mammalian DNA by mll partner tet1. Science 2009; 324: 930–5.

Thompson CL, Drewery DL, Atkins HD, Stephenson FA, Chazot PL. Immunohistochemical localization of n-methyl-d-aspartate receptor nr1, nr2a, nr2b and nr2c/d subunits in the adult mammalian cerebellum. Neurosci Lett 2000; 283: 85–8.

Tomomura M, Rice DS, Morgan JI, Yuzaki M. Purification of purkinje cells by fluorescence-activated cell sorting from transgenic mice that express green fluorescent protein. Eur J Neurosci 2001; 14: 57–63.

West AE. Cocaine shapes chromatin landscapes via tet1. Nat Neurosci 2015; 18: 478–80.

Xu Y, Wu F, Tan L, Kong L, Xiong L, Deng J, et al. Genome-wide regulation of 5hmc, 5mc, and gene expression by tet1 hydroxylase in mouse embryonic stem cells. Mol Cell 2011; 42: 451–64.

Yang Y, Herrup K. Loss of neuronal cell cycle control in ataxia-telangiectasia: a unified disease mechanism. J Neurosci 2005; 25: 2522–9.

Yu H, Su Y, Shin J, Zhong C, Guo JU, Weng YL, et al. Tet3 regulates synaptic transmission and homeostatic plasticity via DNA oxidation and repair. Nat Neurosci 2015; 18: 836–43.

Yu M, Hon GC, Szulwach KE, Song CX, Zhang L, Kim A, et al. Base-resolution analysis of 5-hydroxymethylcytosine in the mammalian genome. Cell 2012; 149: 1368–80.

Zhang L, Lu X, Lu J, Liang H, Dai Q, Xu GL, et al. Thymine DNA glycosylase specifically recognizes 5-carboxylcytosine-modified DNA. Nat Chem Biol 2012; 8: 328–30.